INTERNATIONAL JOURNAL OF AUTOMOTIVE AND MECHANICAL ENGINEERING (IJAME)
ISSN: 2229-8649 e-ISSN: 2180-1606
VOL. 19, ISSUE 4, 2022, 10063 – 10072
DOI: https://doi.org/10.15282/ijame.19.4.2022.03.0777

ORIGINAL ARTICLE

# Passive Flow Control of Ahmed Body using Control Rod

A. Şumnu*

Faculty of Aeronautics and Aerospace Engineering, İskenderun Technical University, 31200 Hatay, Turkey

**ABSTRACT** – In the current study, numerical analysis of passive control flow with a control rod for Ahmed body is performed at different slant angles and velocities and placed rod locations on the slant surface. The aim of the study is to improve aerodynamic performance by preventing flow separation on the slant surface of Ahmed body using a control rod. This passive flow control method uses a control rod that has not been applied for simplified ground vehicles before. Therefore, it can be said that this study is a new example in point of a passive flow control application for Ahmed body. The solution of the study is performed by using the Computational Fluid Dynamics (CFD) method. The solutions are firstly performed for baseline geometry, and the results are compared with experimental data reported in the literature for validation. CFD solutions are carried out by means of the ANSYS and RNG k-ε turbulence model is used to simulate flow-field since it captures the effect of turbulent flow. The solutions used a control rod with a 20 mm diameter performed at a dimensionless location (X/L=0.057 and 0.153) for Ahmed body. The results are presented visually in the figures, and drag coefficient values are also given in Table format. It is concluded that the rod application is useful for some specified slant angles and velocities since flow separation delays and suppresses the slant surface. The maximum drag reduction is achieved at about 6.153% at a slant angle of 35° and 20 m/s velocity of air, and location of control rod of 0.057, while the minimum drag reduction is about 1.048% at slant angle of 25° and velocity of air at 40 m/s and location of control rod of 0.153.

**ARTICLE HISTORY**
Received: 17th Apr. 2022
Revised: 03rd Oct. 2022
Accepted: 21st Dec. 2022
Published: 28th Dec. 2022

**KEYWORDS**
*Ahmed Body;*
*CFD;*
*Drag force;*
*Flow separation;*
*Control rod*

## INTRODUCTION

Drag reduction is a crucial issue in the point of fuel consumption for all moveable vehicles. Most of the drag generally originates from pressure drag that occurs when the layers of air separate away from the surface and begin eddying motion. The aerodynamic efficiency can be increased by controlling flow. For this, passive and active flow control methods can be used to prevent flow separation or swirl flow formation and reduce pressure drag. The passive flow control method can be described as that it is manipulating the flow over the body without exterior energy. In this study, a control rod is used as a passive control device. The control rod has not been applied before for ground vehicles to improve aerodynamic performance. Hence, the objective of this study is to use a control rod for Ahmed body and investigate the flow physics occurring on the slant surface and rear region of the body.

Flow control of the NACA0012 airfoil was performed using active and passive vortex generators at subsonic flow for delaying flow separation by Shan et al. [1]. A numerical investigation of passive control flow was proposed using a static micro-cylinder and oscillating micro-cylinder for the S809 airfoil by Shi et al. [2]. Another study that was performed using passive control with a micro-cylinder device is presented to show differences between controlled and uncontrolled situations using Reynolds Averaged Navier Stokes (RANS) and delayed detected eddy simulation (DDES) [3]. Numerical analysis of flow control was performed for regular shape and bumpy shape airfoils [4]. The study to control flow over wind turbine blade airfoil was implemented using roughness elements, and the pre-stall flow control was achieved [5]. In order to control the flow over a NACA 4415 airfoil, design optimization was performed for the vortex generators [6]. The flow control of a NACA 0012 airfoil was performed using micro-riblet film (MRF), and the experimental studies were performed and compared for both smooth surface and MRF at different air velocities [7]. Passive and active control devices that are contour bump and jet actuators, respectively, were used to reduce drag force, and a gradient-based optimization method was applied to find the optimum design of control devices [8].

Investigation of laminar separation bubble structure and flow characteristic was presented at low Reynolds number, and it was indicated that pressure distributions were affected by chord Reynolds number and some disturbances. So, these should be taken into account when an analytic solution is performed [9]. The observation of laminar bubble separation was also presented for NACA0012 [10]. The experimental study was presented to observe the separated shear layer and wake formation of an airfoil to improve the coherent structure [11]. The experimental study at a low Reynolds number for flow SD7062 airfoil was performed by using a rod. The laminar separation bubble was observed for both cases, which are baseline airfoil and airfoil with a control rod. It was stated that the rod diameter and position on the airfoil were important to suppress or delay the flow separation [12]. Fırat et al. [13] used square-rod to control the flow and it was concluded that the control rod is effective on both reduction of drag force and suppressing the unsteady aerodynamic

*CORRESPONDING AUTHOR | A. Şumnu | ✉ ahmet.sumnu@iste.edu.tr

© The Authors 2022. Published by University Malaysia Pahang Publishing. This is an open access article under the CC BY license.

force. The similar study was presented to control flow past over the square rod at various Reynolds Number by Ahmed et al. [14]. The wind tunnel testing for observation of vortex generation, both active and passive cases were also carried out by Seshagiri et al. [15]. They observed that flow control with an oscillating micro-cylinder was better than the static one. Heffron et al. [16] observed the effect of MVG vane on control flow over the E387 airfoil. The investigation of trip strips was implemented to observe flow separation [17].

In order to suppress flow over an airfoil, dual excitation (Dielectric Barrier Discharge) DBD plasma actuators were used [18]. A similar study was also proposed by performing numerical simulations using multiple DBD plasma actuators [19]. In addition, stationary and non-stationary AC-DBD plasma actuators were used to improve flow over the NACA0024 airfoil [20]. Acoustic flow control for a NACA 2415 airfoil was carried out at low Reynolds number and it was revealed that the acoustic control effect on the separation bubble was decreased while Reynolds number increased [21]. Another study related to controlling the flow in different ways was implemented using a flexible flap for NACA 0012 airfoil. It was inferred that the proposed method provided to increase lift to drag ratio [22]. A similar study investigated a self-adapting flexible flap to control flow over the NACA 0012 was carried out by Hafien et al. [23]. Active flow control was also presented using both suction and blowing methods for NACA 0012 airfoil, and numerical simulation was performed using parameters of suction and blowing that are jet locations, amplitudes and angles [24]. The paper was presented to increase aerodynamic performance by means of protuberances at the leading edge and evaluate the lift and drag forces [25]. The flow control was proposed using the blowing technique and investigated blowing jet amplitude and dimensions to find optimum results in point of aerodynamics [26]. Some flow regulation may be performed with shape modifications to increase aerodynamic performance. Şumnu [27] studied Ahmed body aerodynamics by modifying the shape and reducing the aerodynamic drag coefficient. In addition, different turbulence models were used to perform the solution and find the proper model as RNG k-ε.

The early separated flow or stall generation reduces the performance of an airfoil or a ground vehicle in terms of aerodynamics. Flow separation may especially occur at high Reynolds numbers and slant surfaces for a ground vehicle. This disturbance can be prevented using some active or passive control methods. Flow control can be achieved by a rod placed on the slant surface because flow separation generally occurs in this place. In the literature related to Ahmed body, suggestions of flow control of the rear region of a body using a control rod could not be observed. Hence, the control rod is mounted to the slant surface of the body to delay separation flow in the present study. Ahmed body with a rod placed on the slant surface is performed at different air velocities, slant angles and rod positions to enhance aerodynamic performance. Some previous study on control rod that is applied to an airfoil is mentioned above.

## COMPUTATIONAL METHOD

### Mathematical Model and Numerical Methods

In the presented study, the CFD solution is implemented using Fluent ANSYS (17.2) that uses finite control volume methods. Three-dimensional, steady, incompressible flow analyses are performed using Reynolds Averaged Navier-Stokes equations (RANS). The continuity and momentum equations are available in the Navier-Stokes equations. These are given in the following Eq. (1) and Eq. (2).

$$\frac{\partial \rho}{\partial t} + \vec{\nabla}(\rho \vec{V}) = 0 \tag{1}$$

The Navier-Stokes equation in the x-direction can be written as:

$$\frac{\partial(\rho u)}{\partial t} + \nabla(\rho u V) = -\frac{\partial P}{\partial x} + \frac{\partial \tau_{xx}}{\partial x} + \frac{\partial \tau_{yx}}{\partial y} + \frac{\partial \tau_{zx}}{\partial z} + \rho f x \tag{2}$$

The drag coefficient is an important characteristic of the aerodynamics of vehicles. It can be calculated using the following Eq. (3).

$$C_D = \frac{D}{\frac{1}{2}\rho {V_\infty}^2 S} \tag{3}$$

Re-Normalization Group (RNG) k-ε turbulence model is used to simulate the flow over Ahmed body since it can properly capture the flow field near the boundary layer and gives correct results. The RNG model that is developed by Yakhot et al. [28] is a mathematical technique which is utilized to derive a turbulence model. This method renormalized the Navier-Stokes equations to be able to account for the effect of smaller motion. The transport equation of RNG k-ε can be expressed as following Eq. (4) and Eq. (5).

$$\frac{\partial}{\partial t}(\rho k) + \frac{\partial}{\partial x_i}(\rho k u_i) = \frac{\partial}{\partial x_j}\left[\left(\mu + \frac{\mu_t}{\sigma_k}\right)\frac{\partial k}{\partial x_j}\right] + P_k - \rho\varepsilon \tag{4}$$

$$\frac{\partial}{\partial t}(\rho\varepsilon)+\frac{\partial}{\partial x_i}(\rho\varepsilon u_i)=\frac{\partial}{\partial x_i}\left[\left(\mu+\frac{\mu_t}{\sigma_\varepsilon}\right)\frac{\partial\varepsilon}{\partial x_i}\right]+C_{1\varepsilon}\frac{\varepsilon}{k}P_k+C_{2\varepsilon}^{*}\rho\frac{\varepsilon^2}{k} \quad (5)$$

where,

$$C_{2\varepsilon}^{*}=C_{2\varepsilon}+\frac{C_{\mu\eta^3}\left(1-\frac{\eta}{\eta_0}\right)}{1+\beta\eta^3}$$

$$\eta=Sk/\varepsilon$$

$$S=(2S_{ij}S_{ij})^{1/2}$$

## Geometry of Ahmed body and Computational Set-Up

The Ahmed body dimensions are given in Figure 1(a), adapted from Hinterberger et al. [29] and Ahmed et al. [30]. The geometry of the body is generated using Designmodeler in ANSYS. The solid model of Ahmed body with a rod control device is presented in Figure 1(b). The diameter of the control rod is 20 mm and it is presented in Figure 1(c). In order to perform the solution sufficiently, a computational fluid domain is generated. The width and height of the fluid domain are ten times the body, and its length is twelve times the body. The defined boundary condition is convenient for obtaining accurate results.

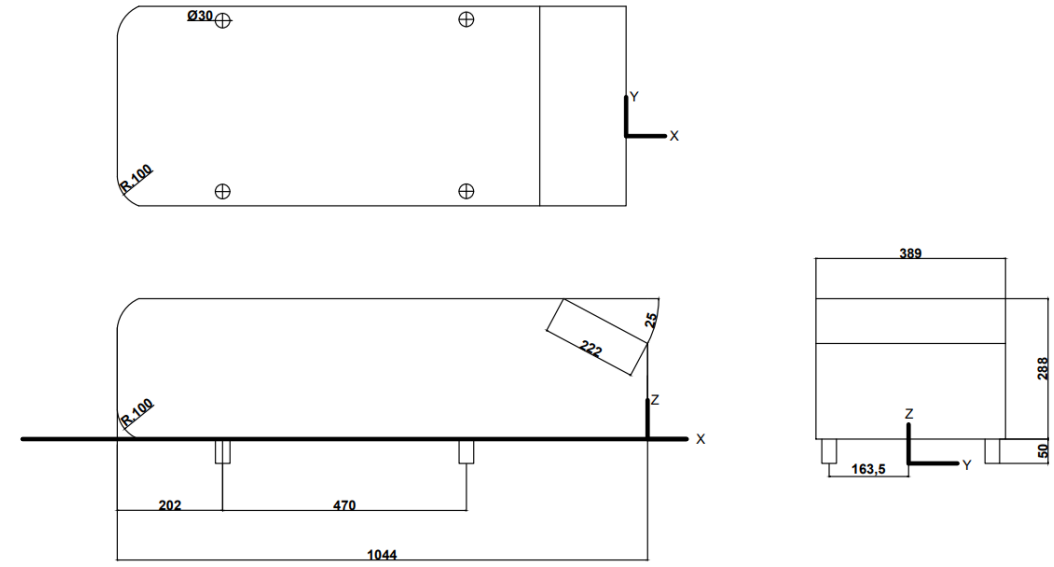


(a)

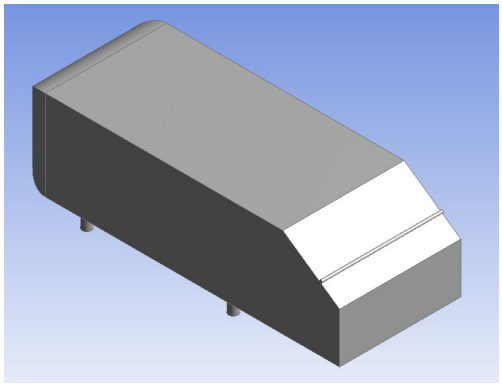

(b)

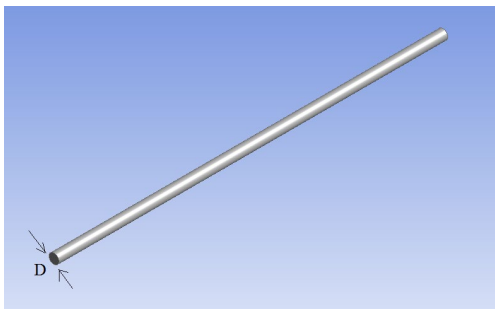


(c)

**Figure 1.** (a) Ahmed body dimensions in mm, (b) Ahmed body with control rod and, (c) control rod

The computational set-up is described in Fluent ANSYS when the CFD solution is performed. The wall-type is selected for Ahmed body and road due to the no-slip condition. The enclosure surfaces are defined as symmetry during the solution. The inlet and outlet plane represent the velocity-inlet and pressure outlet for boundary conditions, respectively. The implicit formulation with Roe-FDS flux type is defined for the solution method. The flow is selected as second-order upwind. The solver type is defined as density-based and steady-state for computation of flow field. The courant number that is a dimensionless number is 0.7 for the solution. It represents the time a particle stays in a cell of mesh. The wall function is selected as an enhancement wall treatment that is a near wall modeling method for RNG k-ε turbulences model. The dimensionless wall distance value is about $y^+\approx1$ to capture the flow-field in the boundary layer.

This value can be greater than "1" somewhere on the body. In addition, the computational run is finished when the residuals are $10^{-5}$ and the change of drag coefficient value is negligibly small.

### Grid Independence and CFD Validation Process

The efficient grid or mesh generation is crucial to solving problems accurately. Therefore, the mesh generation is performed at different numbers that start from courser to the finer grid. In the grid validation process, the mesh generation is carried out ten times and a CFD solution is performed for each of them to find an efficient mesh number. It is concluded that 2,301,000 mesh numbers are sufficient for the solution since CFD solution results were negligible change for higher mesh numbers. The grid independence is shown in Figure 2. The mesh generation is carried out using ANSYS Mesh. The inflation layer is formed over the body using twenty layers and the prismatic mesh is generated near the wall of body. Face sizing is applied to control mesh generation and capture flow. The remaining part of the computational fluid domain is generated hexahedral mesh structure. Mesh generation around the Ahmed body is given in Figure 3.

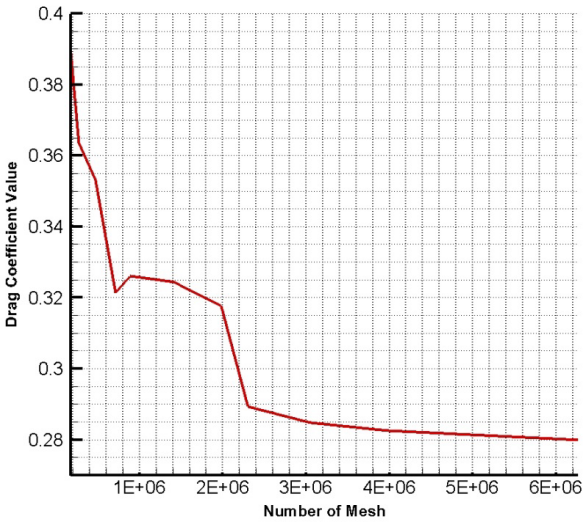


**Figure 2.** Mesh independency for Ahmed body

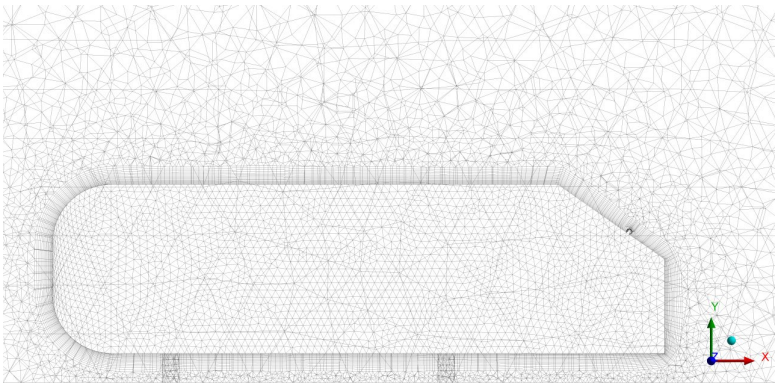


**Figure 3.** Mesh generation around Ahmed Body

The RNG k-ε turbulence method is suitable for ground vehicles since it gives more accurate results. The study of Şumnu [27] investigated different turbulence models to show which one is in good agreement with experimental results. Table 1 shows the drag coefficient values $C_D$ for five different turbulence models and their differences from the experimental result that is reported by Meile et al. [31]. It can be observed that the solution result of RNG k-ε turbulence model is close to the experimental value. In addition, the solution results are compared with both experimental data [31] and CFD results [27] to validate this study at 40 m/s and Reynolds number (length based on body) of $2.78\times10^6$ . Table 2 presents drag coefficient values for body without a control rod. It can be concluded that the solutions are good agreement with experimental results that reported in [31],[32] and differences of $C_D$ values between present study and previous studies [31],[32] are acceptable.

**Table 1.** Drag coefficient values and their differences between experimental results and solutions for selected turbulence models [27]

| Turbulence model | $C_D$ Value | Differences (%) |
|---|---|---|
| Spalart-Allmaras | 0,362 | 29,74 |
| SST k-ω | 0,3401 | 21,89 |
| Standard k-ε | 0,3283 | 17,67 |
| Realizable k-ε | 0,303 | 8,60 |
| RNG k-ε | 0,281 | 0,71 |
| Experimental result [31] | 0,279 | - |

**Table 2.** Comparison of drag values without control rod of the body for validation

| Slant angle | Velocity of air (m/s) | $C_D$ value [31,32] | $C_D$ value (present study) | Differences (%) |
|---|---|---|---|---|
| 25° | 20 | 0.360 [32] | 0.3701 | 2.800 |
| | 40 | 0.299 [31] | 0.2860 | 4.390 |
| 35° | 20 | 0.278 [32] | 0.2909 | 4.430 |
| | 40 | 0.279 [31] | 0.2810 | 0.071 |

## RESULTS AND DISCUSSION

In this study, CFD solution analyses were performed at various velocities, slant angles and location of rod positions. In addition, the solutions were performed with the control rod positioned without contact on the slant surface at various velocities and slant angles. The solution was initially carried out for baseline geometry to compare Ahmed body with the control rod. The diameter of control rod used was 20 mm for all cases. The position of rod was normalized with the length of Ahmed body and two position ratios (X/L= 0.057, 0.153) were examined at slant angles of 25° and 35°. The placements of control rod were determined according to the location of flow separation at the slant surface for baseline geometry.

Figure 4 and 5 show the time averaged streamline topologies at 25° slant angle and both 20 m/s and 40 m/s, respectively. These figures present the solution of the baseline body and control rod at 0.057 and 0.153. When examined Figure 6, it can be observed that flow separation occurs on the slant surface for baseline body, and the zone having negative velocity shows a recirculation region. The separation may occur due to an adverse pressure gradient encountered as the flow expands, causing an extended region of separated flow [33]. The intensity of turbulent flow over the slant surface reduces for the location of control rod of X/L=0.057. When the location of control rod is X/L=0.153, the negative velocity zone can be detected, but the recirculation region disappears on the slant surface. This provides a reduction of drag force on the body.

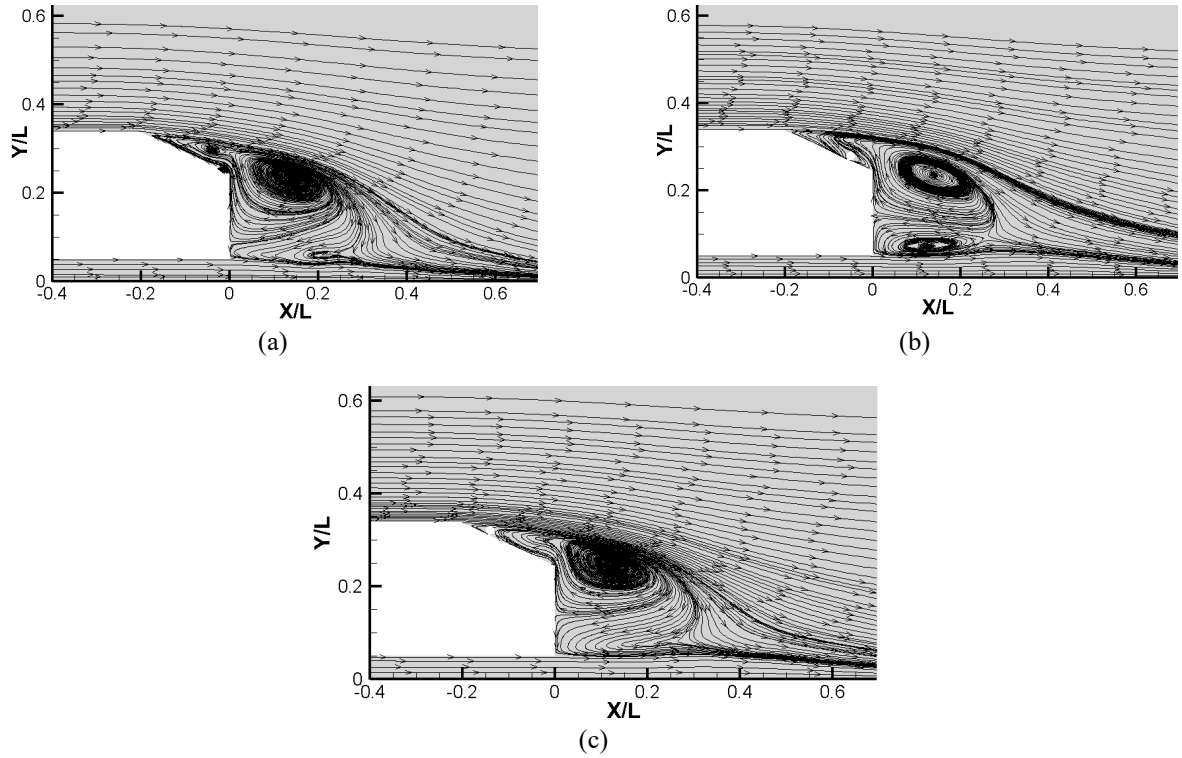


**Figure 4.** Streamlines topologies of Ahmed body at 25° slant angle and 20 m/s: (a) baseline body, (b) control rod position at 0.057, and (c) control rod position at 0.153

In Figure 5, flow separation for baseline geometry at the end of the slant surface eliminates due to the higher velocity of air when compared with Figure 4. However, the vortex generation is observed on the slant surface at approximately X/L=0.057 for baseline geometry. When the solutions for control rod are observed at location of 0.057 and 0.153, the vortex generation reduced on the slant surface.

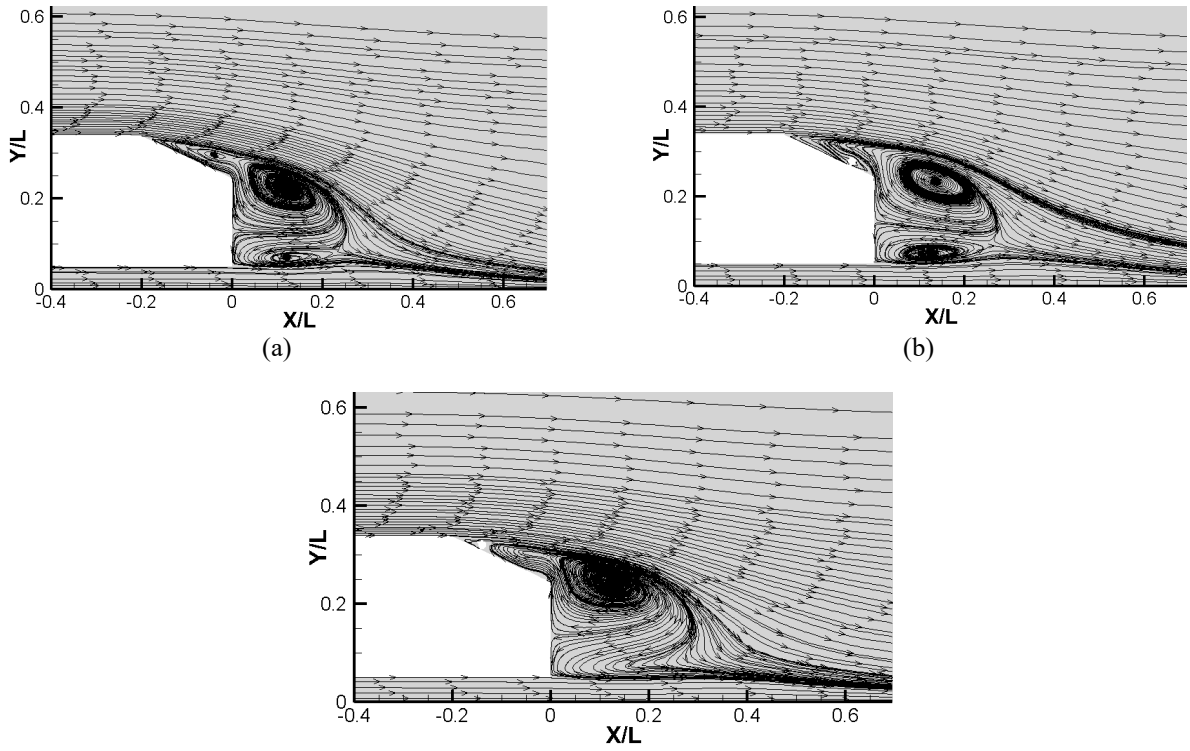


**Figure 5.** Streamlines topologies of Ahmed Body at 25° slant angle and 40 m/s: (a) baseline body, (b) control rod position at 0.057 and (c) control rod position at 0.153

Figures 6 and 7 show the time-averaged streamline topologies at 35° slant angle and both 20 m/s and 40 m/s, respectively. The intensity of recirculation region in baseline body on slant surface of 35° is higher than 25° slant angle. The separation zone is delayed thanks to the control rod for locations of 0.057 and 0.153. However, the negative velocity zone is not eliminated with this method. It can be stated that the effect of control rod is higher for slant angle 35° when compared with slant angle 25°. The height of recirculation zone reduces for solution at 40 m/s due to increased momentum.

In addition, the height of boundary layer and size of vortex generation that occurs rear region of the body was reduced for location X/L=0.057 due to the control rod effect. The other location (X/L=0.153) of control rod for 40 m/s in Figure 7 shows approximately the same situations at the rear region except for the occurrence of recirculation zone at the front that increased drag force. When the drag reduction values are observed between the cases, the control rod doesn't show the same effect for all cases. Table 3 shows the drag coefficient values for body with control rod at slant angles (25° and 35°) and velocities of air (20 and 40 m/s).

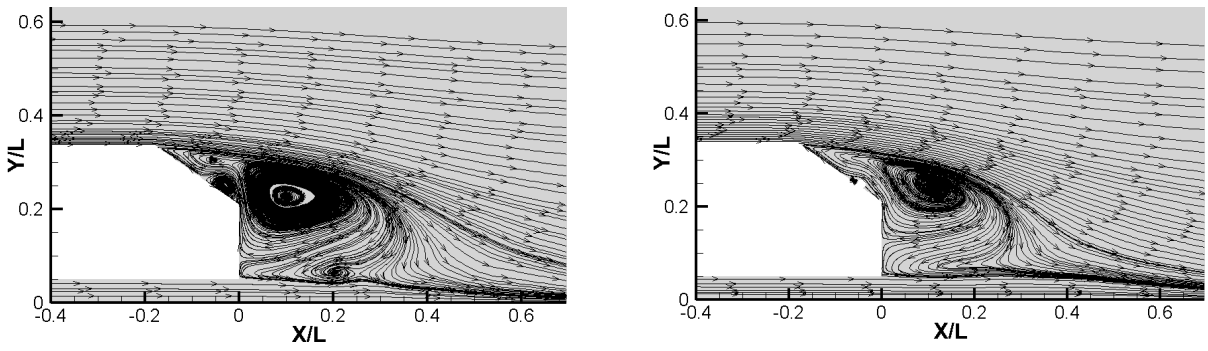

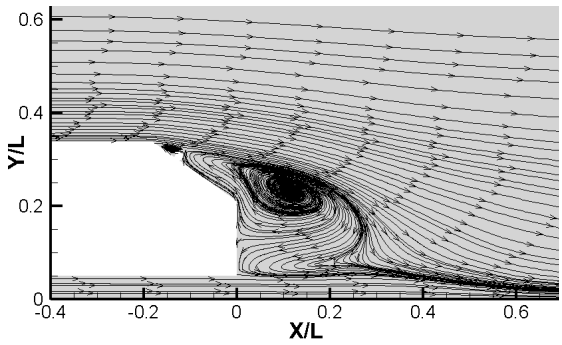


(c)

**Figure 6.** Streamlines topologies of Ahmed Body at 35° slant angle and 20 m/s (a: Baseline body, b: Control rod position at 0.057 c: Control rod position at 0.153)

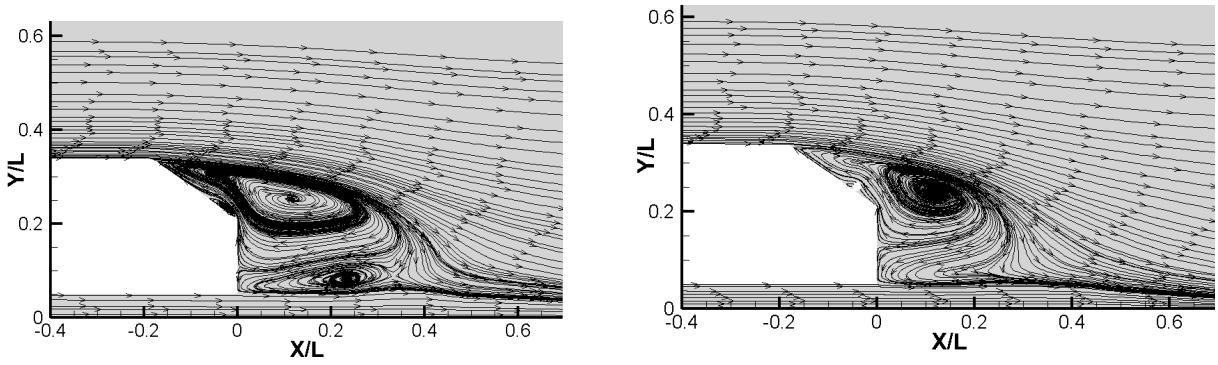


(a) (b)

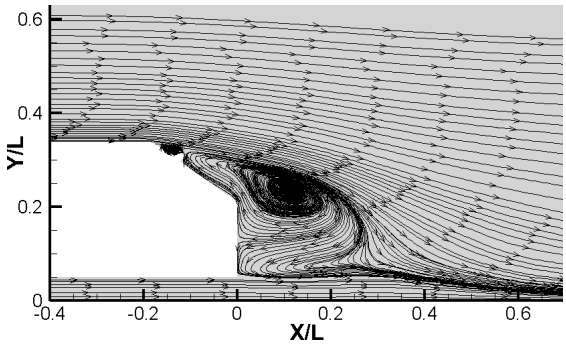


(c)

**Figure 7.** Streamlines topologies of Ahmed Body at 35° slant angle and 40 m/s (a: Baseline body, b: Control rod position at 0.057 c: Control rod position at 0.153)

**Table 3.** Drag coefficient values for body with control rod

| Slant angle | Velocity of air (m/s) | Position of control rod (X/L) | $C_D$ value of body with control rod |
|---|---|---|---|
| 25° | 20 | 0.057 | 0.3607 |
| | | 0.153 | 0.3597 |
| | 40 | 0.057 | 0.2810 |
| | | 0.153 | 0.2830 |
| 35° | 20 | 0.057 | 0.2730 |
| | | 0.153 | 0.2841 |
| | 40 | 0.057 | 0.2695 |
| | | 0.153 | 0.2770 |

The solutions are also performed without contact on slant surface to observe effect of control rod in point of aerodynamic performance. Figures 8 and 9 show the time-averaged streamline topologies for Ahmed body without contact on slant surface at 25° slant angle and both 20 m/s and 40 m/s, respectively. This method prevents separation of flow in the boundary layer at a slant surface of 25° and 20 m/s air velocity for the location of X/L=0.153, while laminar bubble separation occurs on the trailing edge of slant surface for the location of X/L=0.057. In addition, the height of recirculation at the rear region of body for location of control rod (0.153) is reduced. It can be inferred that control rod increases performance at location of X/L (0.153) since the intensity of turbulent flow is reduced when compared with baseline body solution. Figure 9 also shows similar flow characteristics to Figure 8. It can be observed that the recirculation zone on the

slant surface is reduced at 40 m/s, due to an increase in momentum of boundary layer. However, the drag coefficient values are compared with body control rod with contact on slant surface 25° for velocity 20 m/s, the change of aerodynamic performance of the body is negligibly small. Hence, it can be said that this method is not suitable for all conditions.

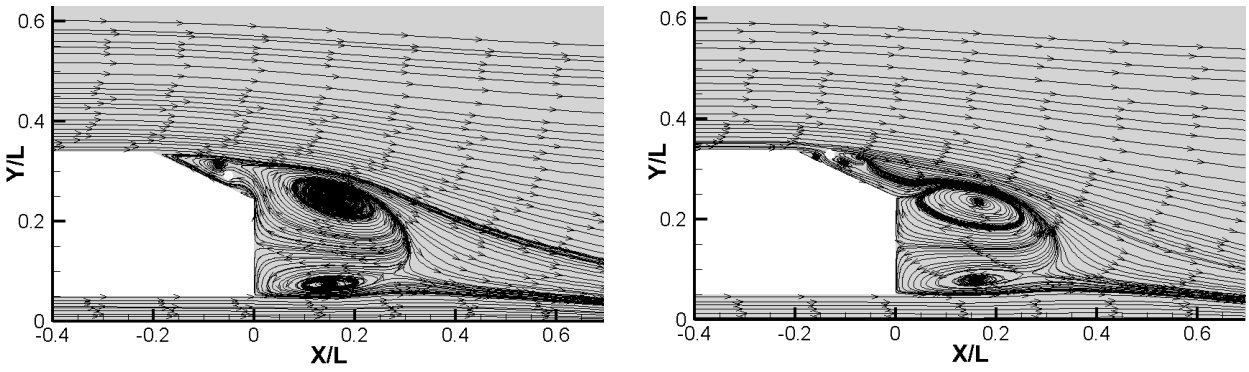


(a) (b)

**Figure 8.** Streamlines topologies of Ahmed Body at 25° slant angle and 20 m/s. Control rod position without contact on slant surface at (a) 0.057 and (b) 0.153

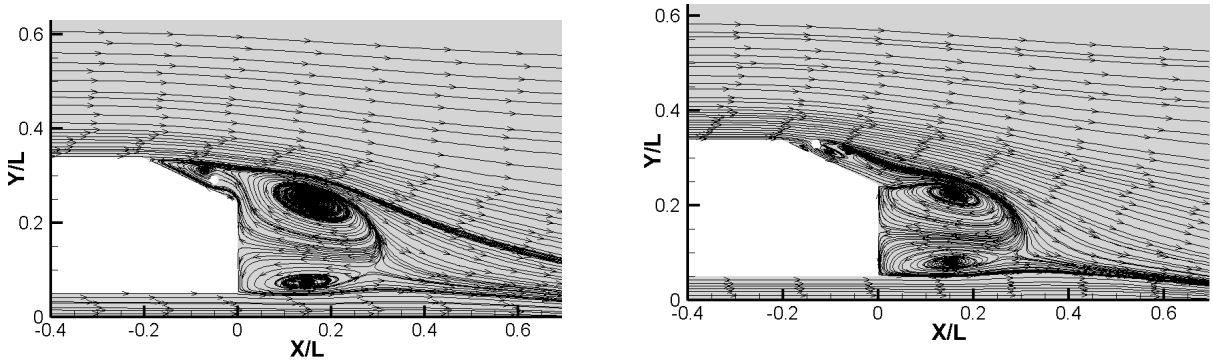


(a) (b)

**Figure 9.** Streamlines topologies of Ahmed Body at 25° slant angle and 40 m/s. Control rod position without contact on slant surface at (a) 0.057 and (b) 0.153

Figure s10 and 11 show the time-averaged streamline topologies for Ahmed body without contact on the slant surface at 35° and both 20 m/s and 40 m/s, respectively. The separation of flow is not observed for solutions that performed at 20 m/s and 40 m/s for location of control rod of X/L=0.057. However, the recirculation zone having two foci occurs on slant surface of body and above the control rod when both Figures 10(a) and 11(a) are observed. For these solutions, the aerodynamic performance improved thanks to preventing flow separation in the boundary layer. The negative velocity zone on slant surface is observed in Figures 10(b) and 11(b). The recirculation size and intensity of turbulent flow reduced when compared with baseline geometry solution at 35° slant angle. Hence, drag reduction is provided using control rod without contact on slant surface when compared with baseline body at 35° slant angle. Table 4 is also presented to show the drag coefficient values of body using control rod without contact on the slant surface (at 25° and 35°) and velocities of air at 20 and 40 m/s.

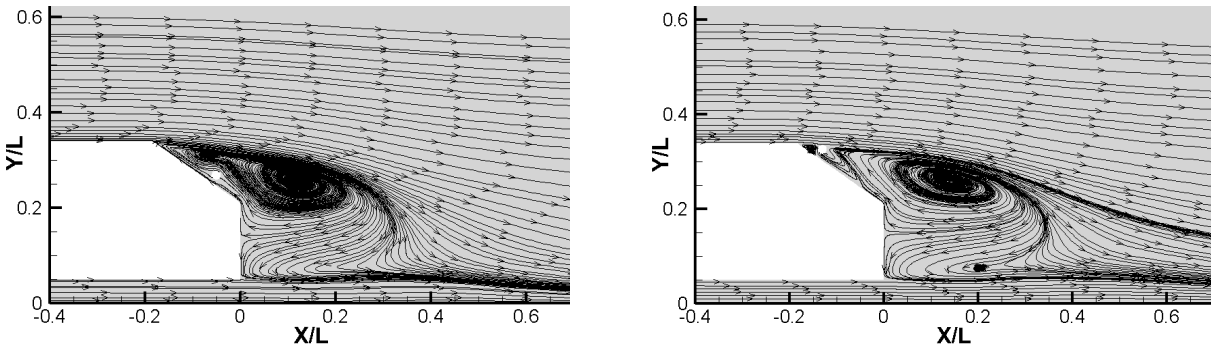


(a) (b)

**Figure 10.** Streamlines topologies of Ahmed Body at 35° slant angle and 20 m/s. Control rod position without contact on slant surface at (a) 0.057 and (b) 0.153

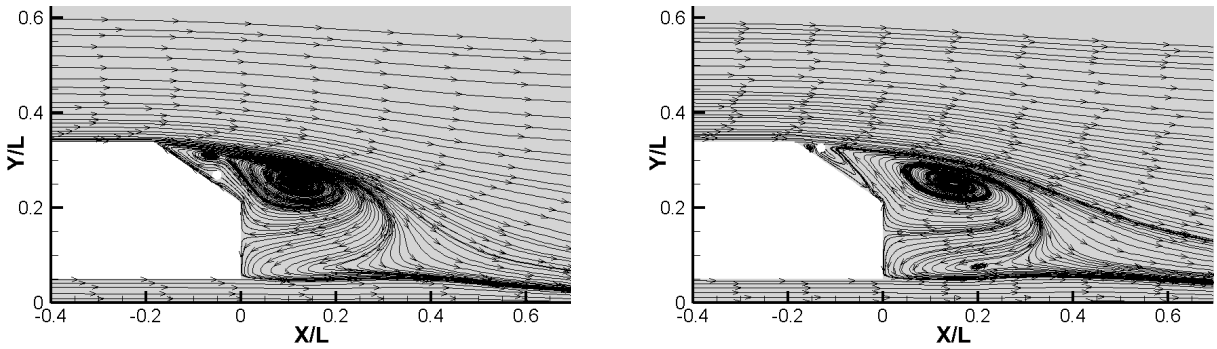


**Figure 11.** Streamlines topologies of Ahmed Body at 35° slant angle and 40 m/s. Control rod position without contact on slant surface at (a) 0.057 and (b) 0.153

**Table 4.** Drag coefficient values for control rod position at without contact on slant surface

| Slant angle | Velocity of air (m/s) | Position of control rod (X/L) | $C_D$ value of body with control rod |
|---|---|---|---|
| 25° | 20 | 0.057 | 0.3780 |
| | | 0.153 | 0.3683 |
| | 40 | 0.057 | 0.2890 |
| | | 0.153 | 0.2880 |
| 35° | 20 | 0.057 | 0.2712 |
| | | 0.153 | 0.2732 |
| | 40 | 0.057 | 0.2756 |
| | | 0.153 | 0.2725 |

## CONCLUSIONS

In this study, the passive flow control with a rod for Ahmed body was performed at different air velocities, slant surface and positions of control rod. The CFD solution was performed for specified cases and results were presented as visually for all cases. The results showed that the recirculation size and laminar bubble separations were prevented and delayed using a control rod. However, some cases could not be applicable in point of aerodynamic performance while some cases gave good results and reduced aerodynamic drag. Thus, the control rod positioned the dimensionless location (X/L=0.057 and 0.153). When examined the drag coefficient values for each case, the maximum drag reduction was achieved at about 6.153% at a slant angle of 35°, 20 m/s velocity of air and location of control rod of 0.057. In addition, the minimum drag reduction was observed at about 1.048% at a slant angle of 25° and velocity of air of 40 m/s and 0.153 location of control rod. The solutions were also conducted the rod without contact on slant surface to investigate flow physics and these solutions showed that flow separation was prevented at location of 0.057 for 35° slant angle.

However, when the comparison of solutions for the control rod with and without contact to slant surface, drag reduction was not significantly observed. The drag value increased at 25° slant angle and 20 m/s, since vortex formation occurred on the control rod and flow separation was observed at the end of slant surface. When observing drag coefficient values for slant angle of 35°, the solution results were more reasonable according to the solution for control rod with contact on slant surface. Finally, when the velocity streamline topologies were observed and compared with baseline geometry, the control rod showed good performance in the point of aerodynamics by preventing flow separation at boundary layer. However, this passive control device may not be applied for all cases and geometry since it didn't indicate good performance in some conditions. The future study using the control rod device can be performed at different rod diameters and applied aerodynamic shape optimization to improve the performance.

## ACKNOWLEDGEMENT

Author would like to thank Aeronautics and Aerospace Engineering Department at Gaziantep University for providing work station.

## REFERENCES

[1] H. Shan, L. Jiang, C. Liu, M. Love, and B. Maines, "Numerical study of passive and active flow separation control over a NACA0012 airfoil," *Computers & Fluids*, vol. 37, no. 8, pp. 975-992, 2008.

[2] X. Shi, S. Xu, L. Ding, and D. Huang, "Passive flow control of a stalled airfoil using an oscillating micro-cylinder," *Computers & Fluids*, vol. 178, pp. 152-165, 2019.

[3] D. Luo, D. Huang, and X. Sun, "Passive flow control of a stalled airfoil using a microcylinder," *Journal of Wind Engineering and Industrial Aerodynamics*, vol. 170, pp. 256-273, 2017.

[4] S. H. A. Faruqui, M. A. Al Bari, M. Emran, and A. Ferdaus, "Numerical analysis of role of bumpy surface to control the flow separation of an airfoil," *Procedia Engineering*, vol. 90, pp. 255-260, 2014.

[5] M. S. Genc, KOCA Kemal, and H. H. Acikel, "Investigation of pre-stall flow control on wind turbine blade airfoil using roughness element," *Energy*, vol. 176, pp. 320-334, 2019.

[6] O. M. Fouatih, M. Medale, O. Imine, and B. Imine, "Design optimization of the aerodynamic passive flow control on NACA 4415 airfoil using vortex generators," *European Journal of Mechanics-B/Fluids*, vol. 56, pp. 82-96, 2016.
[7] S. J. Lee, and Y. G. Jang, "Control of flow around a NACA 0012 airfoil with a micro-riblet film," *Journal of Fluids and Structures*, vol. 20, no. 5, pp. 659-672, 2005.
[8] B. Yagiz, O. Kandil, and Y. V. Pehlivanoglu, "Drag minimization using active and passive flow control techniques," *Aerospace Science and Technology*, vol. 17, no. 1, pp. 21-31, 2012.
[9] M. M. O'meara, and T. J. Mueller, "Laminar separation bubble characteristics on an airfoil at low Reynolds numbers," *AIAA Journal*, vol. 25, no. 8, pp. 1033-1041, 1987.
[10] K. Rinoie, and N. Takemura, "Oscillating behaviour of laminar separation bubble formed on an aerofoil near stall," *The Aeronautical Journal*, vol. 108, no. 1081, pp. 153-163, 2004.
[11] S. Yarusevych, P. E. Sullivan, and J. G. Kawall, "On vortex shedding from an airfoil in low-Reynolds-number flows," *Journal of Fluid Mechanics*, vol. 632, pp. 245-271, 2009.
[12] T. Durhasan, "Passive flow control over an airfoil by control rod at low Reynolds number," *Journal of Applied Fluid Mechanics*, vol. 13, no. 6, 2020.
[13] E. Fırat, Y. E. Akansu, and H. Akilli, "Flow past a square prism with an upstream control rod at incidence to uniform stream," *Ocean Engineering*, vol. 108, pp. 504-518, 2015.
[14] A. Ahmed, R. Manzoor, S. U. Islam, and H. Rahman, "Numerical investigation for flow over a square rod through a passive control method at various Reynolds numbers," *Canadian Journal of Physics*, vol. 98, no.5, pp. 425-432, 2020.
[15] A. Seshagiri, E. Cooper, and L. W. Traub, "Effects of vortex generators on an airfoil at low Reynolds numbers," *Journal of Aircraft*, vol. 46, no. 1, pp. 116-122, 2009.
[16] A. Heffron, J. J. Williams, and E. J. Avital, E. J., "Flow seperation and passive flow control on e387 airfoil. In 54th AIAA Aerospace Sciences Meeting, 2016, p. 0324.
[17] L. W. Traub, "Experimental investigation of the effect of trip strips at low Reynolds number," *Journal of Aircraft*, vol. 48, no. 5, pp. 1776-1784, 2011.
[18] A. Ebrahimi, and M. Hajipour, "Flow separation control over an airfoil using dual excitation of DBD plasma actuators," *Aerospace Science and Technology*, vol. 79, pp. 658-668, 2018.
[19] R. Khoshkhoo, and A. Jahangirian, "Numerical simulation of flow separation control using multiple DBD plasma actuators," *Journal of Applied Fluid Mechanics*, vol. 9, no. 4, pp. 1865-1875, 2016
[20] G. Tathiri, H. Parishani, S. G. Pouryoussefi, E. Esmaeilzadeh, S. M. Mirsajedi *et al.*, "Experimental investigation of separation control on a NACA0024 airfoil using stationary and non-stationary AC-Dielectric barrier discharge plasma actuator," *Journal of Applied Fluid Mechanics*, vol. 9, no.2, pp. 877-888, 2016.
[21] M. S. Genç, I. Karasu, H. H. Açıkel, M. T. Akpolat, and G. Özkan, "Acoustic control of flow over NACA 2415 aerofoil at low Reynolds numbers," *Journal of Aerospace Engineering*, vol. 29, no. 6 pp. 04016045-1-19, 2016.
[22] Z. Fang, C. Gong, A. Revell, G. Chen, A. Harwood, and J. O'connor, "Passive separation control of a NACA0012 airfoil via a flexible flap," *Physics of Fluids*, vol. 31, no. 10, p. 101904, 2019.
[23] C. Hafien, A. Bourehla, and M. Bouzaien, "Passive separation control on a symmetric airfoil via elastic-layer," *Journal of Applied Fluid Mechanics*, vol. 9, no. 5, pp.2569-2580, 2016.
[24] L. Huang, P. G. Huang, R. P. LeBeau, and T. Hauser, "Numerical study of blowing and suction control mechanism on NACA0012 airfoil," *Journal of Aircraft*, vol. 41, no. 5, pp. 1005-1013, 2004.
[25] P. W. Weber, L. E. Howle, M. M. Murray, and D. S. Miklosovic, "Computational evaluation of the performance of lifting surfaces with leading-edge protuberances," *Journal of Aircraft*, vol. 48, no. 2, pp. 591-600, 2011.
[26] K. Yousefi, and R. Saleh, "The effects of trailing edge blowing on aerodynamic characteristics of the NACA 0012 airfoil and optimization of the blowing slot geometry," *Journal of Theorical and Applied Mechanics*, vol. 52, pp. 165-179, 2014.
[27] A. Şumnu, "Shape modification of Ahmed body to reduce drag coefficient and determination of turbulence model," *Niğde Ömer Halisdemir Üniversitesi Mühendislik Bilimleri Dergisi*, vol. 10, no. 2, pp. 824-832, 2021.
[28] V. Yakhot, S. A. Orszag, S. Thangam, T. B. Gatski, and C. G. Speziale, "Development of turbulence models for shear flows by a double expansion technique," *Physics of Fluids A: Fluid Dynamics*, vol. 4, no. 7, pp. 1510-1520, 1992.
[29] C. Hinterberger, M. Garcia-Villalba, and W. Rodi, "Large eddy simulation of flow around the Ahmed body," in *The aerodynamics of heavy vehicles: trucks, buses, and trains.*, R. McCallen, F. Browand, J. Ross, Eds. Berlin, Heidelberg: Springer, 2004, pp. 77-87.
[30] S. R. Ahmed, G. Ramm, and G. Faltin, "Some salient features of the time-averaged ground vehicle wake," *SAE Transactions*, vol.93, pp. 473-50, 1984.
[31] W. Meile, G. Brenn, A. Reppenhagen, B. Lechner, and A. Fuchs, "Experiments and numerical simulations on the aerodynamics of the Ahmed body," *CFD letters*, vol. 3, no.1, pp. 32-39, 2011.
[32] B. Mohammadikalakoo, P. Schito, and M. Mani, "Passive flow control on Ahmed body by rear linking tunnels," *Journal of Wind Engineering and Industrial Aerodynamics*, vol. 205, p. 104330, 2020.
[33] D. C. Wilcox, *Basic Fluid Mechanics.* 3rd ed. Mill Valley: DCW Industries, Inc., 2007.